Journal of Dispersion Science and Technology

ISSN: 0193-2691 (Print) 1532-2351 (Online) Journal homepage: https://www.tandfonline.com/loi/ldis20

Synthesis of iron oxide nanoparticles for DNA purification

László Vanyorek, Ágnes Maria Ilosvai, Emma Szőri-Dorogházi, Csaba Váradi, Ferenc Kristály, Ádám Prekob, Béla Fiser, Tamás Varga, Zoltán Kónya & Béla Viskolcz

To cite this article: László Vanyorek, Ágnes Maria Ilosvai, Emma Szőri-Dorogházi, Csaba Váradi, Ferenc Kristály, Ádám Prekob, Béla Fiser, Tamás Varga, Zoltán Kónya & Béla Viskolcz (2019): Synthesis of iron oxide nanoparticles for DNA purification, Journal of Dispersion Science and Technology, DOI: 10.1080/01932691.2019.1708380

To link to this article: https://doi.org/10.1080/01932691.2019.1708380

Published online: 30 Dec 2019.

Submit your article to this journal

Article views: 94

View related articles

View Crossmark data

Full Terms & Conditions of access and use can be found at
https://www.tandfonline.com/action/journalInformation?journalCode=ldis20

JOURNAL OF DISPERSION SCIENCE AND TECHNOLOGY
https://doi.org/10.1080/01932691.2019.1708380

Taylor & Francis
Taylor & Francis Group

Check for updates

Synthesis of iron oxide nanoparticles for DNA purification

László Vanyorek[a], Ágnes Maria Ilosvai[a], Emma Szőri-Dorogházi[a], Csaba Váradi[a], Ferenc Kristály[b], Ádám Prekob[a], Béla Fiser[a,c], Tamás Varga[d], Zoltán Kónya[d], and Béla Viskolcz[a]

[a]Institute of Chemistry, University of Miskolc, Miskolc-Egyetemváros, Hungary; [b]Institute of Mineralogy and Geology, University of Miskolc, Miskolc-Egyetemváros, Hungary; [c]Ferenc Rákóczi II, Transcarpathian Hungarian Institute, Beregszász, Ukraine; [d]Department of Applied and Environmental Chemistry, University of Szeged, Szeged, Hungary

ABSTRACT

Sonochemistry in combination with a combustion procedure was used to prepare superparamagnetic iron oxide nanoparticles. Two different iron precursors, ferrocene and iron(II)-acetate were dispersed in polyethylene-glycol (PEG) with different molecular weight (200–1000) by using a high efficiency ultrasonic technique. The sonochemical treatment initiated the precipitation of iron-hydroxide particles, then the PEG based colloids were burnt to create the iron oxide nanoparticles. Three phases were observed in the samples, magnetite (Fe_3O_4), hematite (α-Fe_2O_3), and maghemite (γ-Fe_2O_3) and their ratio can be modified by changing the iron precursor and the type of PEG. Elektrokinetic (Zeta) potential and the particle size of the synthesized iron oxide nanoparticle samples were measured and the one (A1) based on iron(II)-acetate and PEG200 have been selected to test in DNA purification, because it has negative and small size distribution. The synthesized superparamagnetic nanoparticles have been used successfully in biological isolation (DNA, deoxyribonucleic acid purification), and thus, the developed synthetic procedure is more than suitable for such applications.

GRAPHICAL ABSTRACT

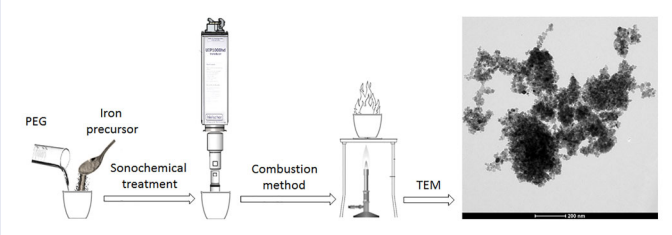

HIGHLIGHTS

- Sonochemical-combustion method was used to synthesize superparamagnetic nanoparticles.
- Magnetite, hematite and maghemite nanoparticles were synthesized.
- The ratio of the iron oxide phases can be tuned by changing the precursors.
- High molecular weight PEG promote the formation of maghemite and hematite.
- High molecular weight PEG inhibits the formation of magnetite.
- The prepared nanoparticles are applicable for DNA purification.

ARTICLE HISTORY
Received 19 September 2019
Accepted 15 December 2019

KEYWORDS
Superparamagnetic; iron-oxide; deoxyribonucleic acid; combustion; sonochemistry; PEG

Introduction

Superparamagnetic iron oxide nanoparticles such as magnetite (Fe_3O_4), hematite (α-Fe_2O_3), and maghemite (γ-Fe_2O_3) and their applications are widely studied in recent literature.[1–9] Iron oxide nanoparticles have been synthesized by Singh et al. using direct conjugation with ginsenosides.[1] Fe_3O_4 and γ-Fe_2O_3 were prepared using a coprecipitation procedure.[2] Iron-oxide nanoparticles with well controlled size and morphology were obtained also by thermal decomposition.[3] Hydrothermal and solvothermal techniques were used to synthesize different nanostructured iron-oxides at a wide range of temperature (130–250 °C) and pressure (0 and 3–4 MPa).[4] Wongwailikhit et al. prepared Fe(III) oxide from microemulsions.[10] Nanoparticles can also be produced with biosynthesis, using iron reducing bacteria.[11] Furthermore, various electrochemical methods have also been tested to prepare iron oxide nanoparticles.[12–14]

Magnetic nanoparticles (MNP) are used in photocatalysis[15] and to build supercapacitators.[16] Core-shell

CONTACT László Vanyorek kemvanyi@uni-miskolc.hu Institute of Chemistry, University of Miskolc, Miskolc-Egyetemváros, Hungary.
Color versions of one or more of the figures in the article can be found online at www.tandfonline.com/ldis.
© 2019 Taylor & Francis Group, LLC

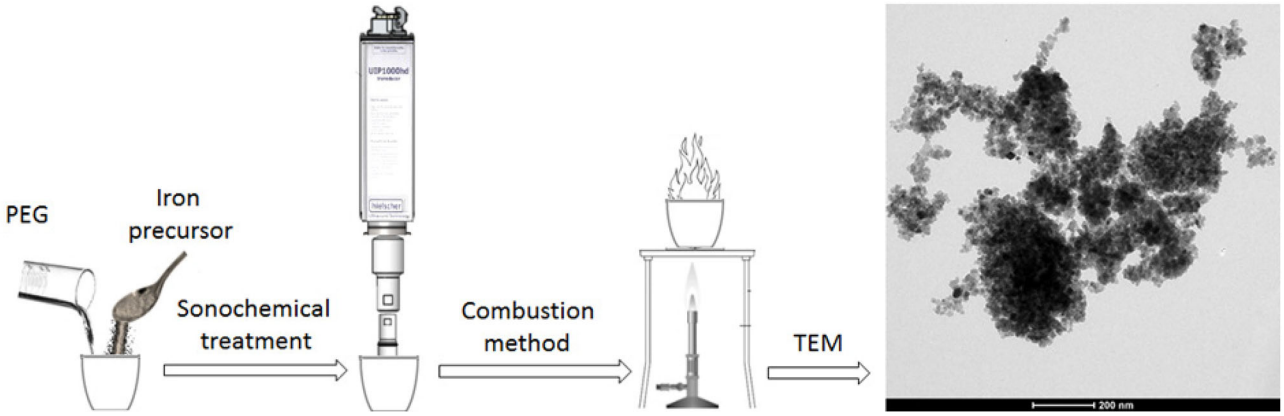

Figure 1. Preparation of superparamagnetic iron-oxide nanoparticles using a combined sonochemical-combustion synthetic procedure.

structured Fe_3O_4-polydopamine nanoparticles were successfully tested to remove heavy metal ions from wastewater.[17] Maghemite nanoparticles and carbon composites have been created to decrease the nitrogen content of fuel oil.[18]

Iron-oxide nanoparticles thanks to their superparamagnetic properties, have a wide range of biomedical applications such as MR imaging,[19,20] and hypothermal treatment of cancer.[21] Furthermore, PEG (polyethylene glycol) coated Fe_3O_4 nanoparticles were made for drug delivery purposes.[22] To increase the biocompatibility of these nanoparticles various polymers have been added to their surface.[23,24] Functionalized nanoparticles have been created and applied to isolate plasmid DNA.[25] DNA purification is still time consuming and chemically demanding procedure. Commonly used centrifuge- and column-based protocols require specialized equipment, often applying toxic reagents, and are not economically scalable or practical to use in a high-throughput manner. The application of magnetic beads can provide an elegant answer to these issues.[26] Various functionalization steps can be applied to modify the surface of magnetic nanoparticles with silica, aminosilane, ionic liquid (1-hexyl-3-methylimidazolium-bromide) and functionalization by carboxyl groups[27–30] and thus, make them applicable in purification procedures. However, the above-mentioned modification steps are time-consuming and costly. Although, conventional Fe_3O_4 have also been used to isolate genomic DNA from mammalian cells.[31] DNA was efficiently bound directly to the magnetite surface, despite that the nanoparticles were not functionalized. The lack of modification steps makes the method simple, quick, cheap, and robust, and it does not require the use of organic solvents. However, the synthetized magnetite was not characterized, the size distribution and electro-kinetic potential of the nanoparticles is unclear.

In this research our goal was to combine two different types of synthesis methods (sonochemistry and combustion) to produce iron oxide nanoparticles with different phase compositions. Furthermore, the applicability of the special synthetized magnetic nanoparticles in DNA purification have been examined, without functionalization of the particles, to avoid the enhanced cost of production.

Materials and methods

Materials

Two different iron precursors, ferrocene (FeC_2O_4, Alfa Aesar) and iron(II) acetate ($Fe(CO_2CH_3)_2$, Sigma Aldrich), were used to synthesize iron oxide nanoparticles. As colloid stabilizing agent and reducing material polyethylene glycol (PEG, Sigma Aldrich) with three different molecular weight (200, 600 and 1000) were applied.

Characterization techniques of the nanoparticles

All synthesized samples were examined by high-resolution transmission electron microscopy (HRTEM, FEI Technai G2 electron microscope, 200 kV), to explore the morphology, particle size and structure of the produced iron oxide nanoparticles. The specimens were prepared by dropping aqueous suspension of the samples on 300 mesh copper grids (Ted Pella Inc.). The diameters of the nanoparticles were measured on the HRTEM images, based on the original scale bar using the *ImageJ* software. X-ray diffraction (XRD) measurements were used to identify and quantify the crystalline phases. Bruker D8 Advance diffractometer (Cu-Kα source, 40 kV and 40 mA) in parallel beam geometry (Göbel mirror) with Vantec1 detector was applied to perform the XRD measurements. Functional groups on the surface of the nanoparticles was studied by Fourier transformed infrared spectroscopy (FTIR) by means of Bruker Vertex 70 spectrometer. All samples were measured in potassium bromide pellets (10 mg sample in 250 mg KBr). The electrokinetic (Zeta) potential of the colloidal systems was measured by Malvern Nano Zs Zetasizer based on electrophoretic mobility (laser doppler electrophoresis). The carbon content of the iron oxides was measured by Vario Macro CHNS element analyzer. The certified phenanthrene standard (C: 93.538%, H: 5.629%, N: 0.179%, S: 0.453%) which was used for the CHNS element analysis purchased from Carlo Erba Inc. (catalogue number: 338 37520). The prepared samples were loaded into tin foils. The carrier gas was helium (99.9990%) while oxygen (99.995%) was used for oxidation.

Synthesis of the superparamagnetic iron-oxide nanoparticles

Two methods were combined to produce magnetic iron oxide nanoparticles (Figure 1). In the first step sonochemical treatment was applied and the iron precursor mixed with the stabilizer (PEG) by using Hielscher UIP1000hdt tip ultrasonic homogenizer for 10 min (340 W/19.4 kHz). After that, the obtained iron-containing colloid was heated and combusted using a Bunsen burner. Then, the combustion has been ceased and the final product cooled to room temperature.

The quantity of iron was kept to 0.642 g in each case (Table 1). The same amount (20 g) of dispersant was used in each experiment. In the case of the A3, B3, and C3 samples the PEG1000 has been warmed up, because this polyol is solid at room temperature.

Nucleic acid isolation and testing DNA binding capacity of the magnetic nanoparticles

In nucleic acid isolation and binding capacity tests a high copy number vector is worthy to use due to the high signal-to-noise ratio, therefore pBAD type vector DNA have been used in our experiments. For initial plasmid preparation *Escherichia coli* (*E. coli*) culture was grown from single colony picked from a freshly streaked plate. This single colony was used to inoculate 5 ml of Luria Bertani (LB) medium and then this starter culture was incubated for 12–16 h at 37 °C with vigorous shaking in a suitable incubator.

Isolation of a plasmid DNA from overnight *E. coli* culture was performed by using the E.Z.N.A. Plasmid DNA Mini Kit procedure based on the manufacturer recommendations (Figure 2A).

To test the nucleic acid binding capacity of the superparamagnetic iron oxide nanoparticles (MNP) a slightly modified Bio-On-Magnetic-Beads method was carried out[26] (Figure 2B). The binding buffer contained the following chemicals in aqueous solution: NaCl (2.5 M), Tris-HCl pH 8.0 (10 mM), EDTA (1 mM), PEG 1540 (20 w/v %), and Tween 20 (0.05 v/v%).

DNA solution was mixed with 20 mg/ml dispersion of the MNPs to achieve 1.8 MNP:DNA ratio. Then 2.5 volume unit of binding buffer was added to one unit of DNA-MNP mixture. The samples were shaken at room temperature for 5 min. MNP (with the bound DNA) was separated by a magnetic stand, and the supernatant with non-binding DNA molecules and other contaminants was discarded. DNA coated magnetic particles were washed with 80 v/v% ethanol for two times. then, the DNA was eluted with highly purified water while MNP particles remain bounded to the magnetic stand. After separation from MNP particles, pure DNA solution was analyzed using agarose gel electrophoresis.

To test the success of reversible DNA-MNP binding, gel electrophoresis experiments have been carried out by using 1.0 w/v% agarose gels with 1× Tris-Acetate-EDTA (TAE) puffer. Mini Sub-Cell GT (Bio-Rad) system was used with a 0.75 cm gel thickness (7 cm × 7 cm) and at 90 V voltage. Electrophoresis was performed until the front edge of the bromophenol blue tracking dye had migrated to a point that was 70% down the gel. Gel loading dye was made at 6× concentration (0.25% bromophenol blue and 30% glycerol). All chemicals used in nucleic acid isolation and testing the DNA binding capacity of the magnetic nanoparticles were purchased from VWR International Ltd.

Table 1. The quantities of the reactants used in the iron oxide nanoparticle preparation.

Sample id.	Precursor	Precursor weight (g)	Dispersant	Dispersant weight (g)
A1	$Fe(CO_2CH_3)_2$	2.00	PEG 200	20.00
A2			PEG 600	
A3			PEG 1000	
B1	FeC_2O_4	2.14	PEG 200	20.00
B2			PEG 600	
B3			PEG 1000	

Results and discussions

Size distribution of iron oxide nanoparticles

The particle size distribution of the produced iron oxide nanoparticles was analyzed (Figure 3A). Smaller particles were formed when iron(II) acetate was used as precursor (Figure 3B). The mean diameter was 15.3 nm, the minimum and maximum particle size was 5.3 nm and 39.8 nm, respectively, in case of the A1 sample within which PEG 200 was used as dispersant. By increasing the molecular weight of the dispersant, the particle size distribution shifted toward the larger values. In case of the PEG600 and PEG1000, the mean sizes are 17.2 nm and 39.6 nm, the minimum 6.9 nm and 21 nm, while the maximum 54.5 nm 131.6 nm, respectively.

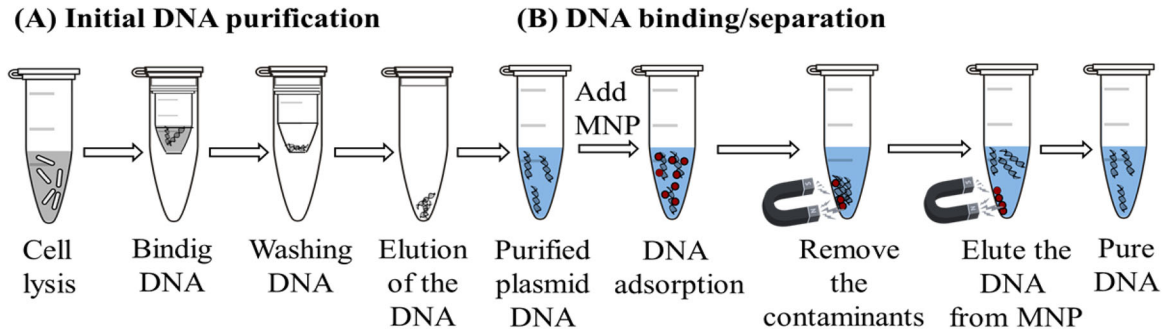

Figure 2. Initial DNA purification (pBAD type plasmid DNA purification from *E. coli* cells) (A); Method for DNA separation from MNPs (B).

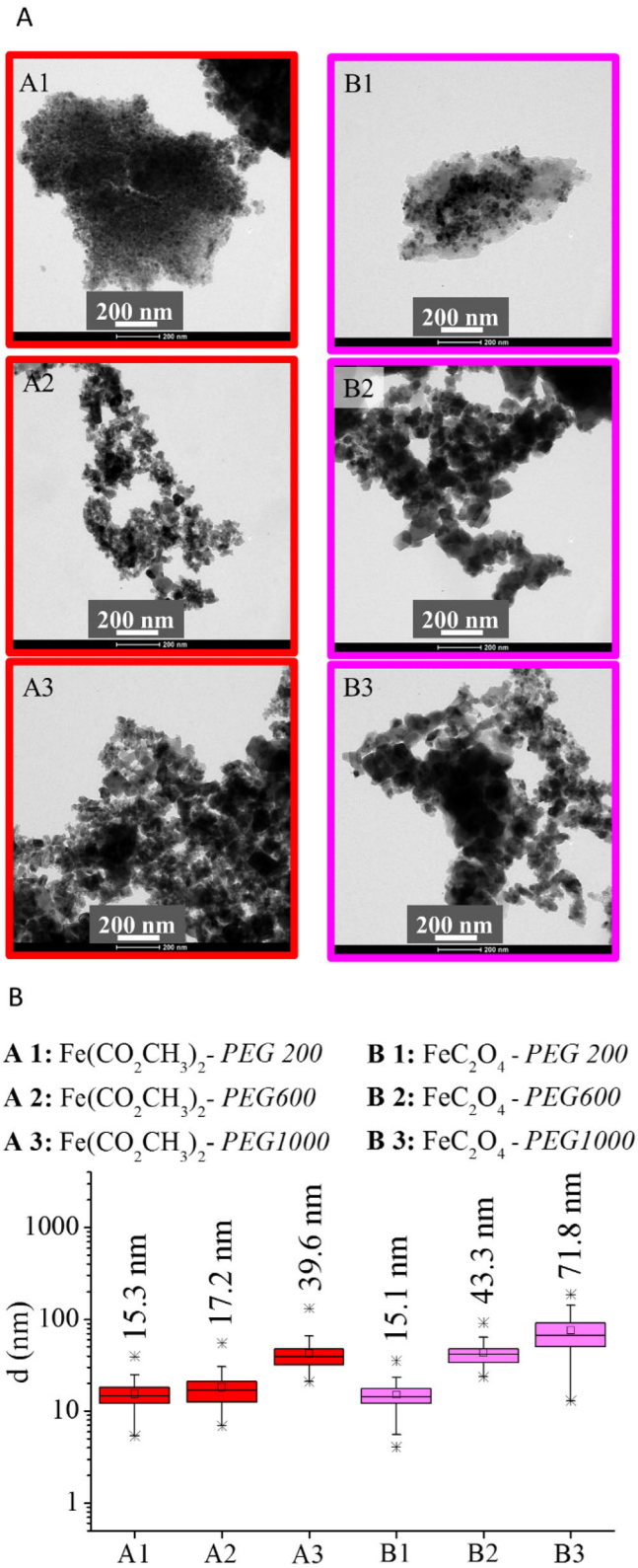

Figure 3. High-resolution transmission electron microscopy (HRTEM) images (A) and particle size distributions (B) of the synthesized iron oxide nanoparticles.

Ferrocene has similar effect as it increase the particle size whenever it is used for the synthesis compared to other precursors. The average diameter of particles in sample B1 (dispersant: PEG200), was 15.1 nm, the size of the smallest particle was 4.1 nm, while the maximum diameter was 35.1 nm. PEG600 and PEG1000 further increased the size of the particles as the average particle sizes are 43.3 nm and 71.8 nm, the minimum 23.6 nm and 27.7 nm, while the maximum 91.3 nm and 185 nm, respectively.

X-ray diffraction (XRD) of the iron oxide particles

The XRD data was evaluated using the Diffrac^{Plus} EVA based on ICDD PDF4 (2016) database. The quantitative phase and size information was extracted by Rietveld refinement in TOPAS4 using size-strain modeling. Three crystalline forms of iron oxides were identified (Figure 4). Characteristic peaks of hematite, magnetite, and maghemite were found. (012), (104) (110), (024), (116), (214), (300) Miller indices indicate that hematite is present in the samples. The following six peaks, (220), (311), (400), (422), (511), and (440) can be assigned to magnetite, while (210), (220), (311), (400), (422), (511), and (440) suggests the presence of maghemite.

Each sample in the B series, contain at least two phases of iron oxides, magnetite and maghemite (Figure 4B). According to the reflexions, hematite only appears in B3.

Quantitative distribution of phases obtained after size-strain modeling is shown in Table 2. In case of the A series (precursor: iron(II)-acetate), the biggest portion is maghemite (γ-Fe_2O_3, 50–80 wt%). The magnetite content is four times higher in sample A1 (28 wt%) than in the other two (7–8%). By increasing the molecular weight of the dispersant, the amount of magnetite decreased, while Fe_2O_3 increased.

Ferrocene has a positive effect on the magnetite formation, as B1 contain more magnetite, than in any of the samples in the A series. The increasing molecular weight of PEG hampered the formation of Fe_3O_4. Hematite was not found in B1 and B2. To summarize, high molecular weight polyethylene-glycols promote the formation of Fe_2O_3 crystal types (maghemite and hematite), and at the same time inhibits the formation of magnetite.

Average crystallite size of the domains calculated by the mean column length calibrated method using full width at half maximum (lowest) and the width of Lorentzian component (highest) of the fitted profiles (Table 2). The particles in the magnetite phase are in the range of 10–30 nm, except for sample A3 (100–170 nm). The size distributions of maghemite particles are similar in the A series of samples (10–30 nm). Only a small amount of hematite particles can be found in the A1 sample (4%), which are quite big 178–280 nm, but these were not detected on the HRTEM image (Figure 5).

In the B series of samples, the size of the magnetite particles is about 10–30 nm, while the diameter of maghemite particles is somewhat wider 19–74 nm. In the B3 sample, there are a few larger hematite particles (>120 nm), and on the HRTEM images particles as big as 185 nm were also detected. The different sized nanoparticles were identified on the HRTEM images based on the XRD analysis (Figure 5). The XRD and HRTEM analysis provided crystallite size information in agreement with each other.

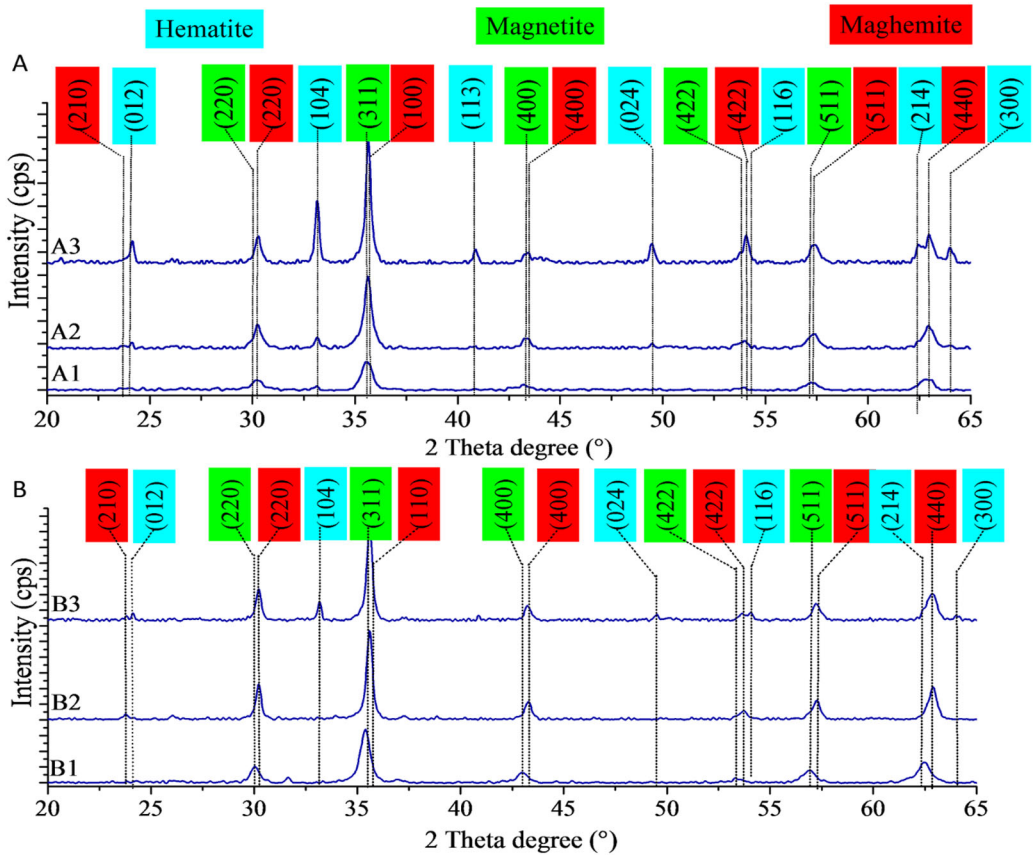

Figure 4. X-ray diffraction (XRD) patterns of the iron oxide nanoparticle samples A1, A2, A3 (A), and B1, B2, B3 (B).

Table 2. The size and phase composition of the iron oxide nanoparticle samples based on X-ray diffraction (XRD) data.

	Mean size of particles (nm)				Phases of iron oxides (%)		
		Particles size based on XRD			Based on XRD measurements		
Sample id.	Range of particles size by SEM	Fe_3O_4	γ-Fe_2O_3	α-Fe_2O_3	Fe_3O_4	γ-Fe_2O_3	α-Fe_2O_3
A1	5–40	13–21	11–17	178–280	28	68	4
A2	7–55	12–19	17–27	40–64	7	82	11
A3	21–132	106–168	16–26	53–84	8	51	41
B1	4–35	12–19	19–30	–	79	21	–
B2	24–91	18–28	34–53	–	30	70	–
B3	13–185	12–19	46–74	81–129	25	60	15

Characterization of the iron oxide nanoparticles

A nanoparticle based reproducible DNA purification method requires stable aqueous dispersion of nanoparticles. Electrokinetic (Zeta) potential provides such information about the electrostatic stability of the particles in aqueous phase. As Figure 6A shows, the Zeta potential values are smaller than −10 mV in case of all samples which is the threshold for aggregation.

Due to the thermal decomposition of PEG, carboxyl (–COOH), and carbonyl (C = O) functional groups can be formed on the surface of nanoparticles. CHNS element analysis of the MNP showed only a small carbon content (e.g. A1 sample 5.4 wt%), therefore bands for carboxyl (–COOH), carbonyl (C = O) are not visible on the FTIR spectra of Figure 6B. The residual carbon content lead to the appearance of three band on the spectrum at 1632, 2854, and 2926 cm^{-1}, which can be attributed to the $\nu C=C$, $\nu_{as}CH$, $\nu_{s}CH$ vibration. Stretching vibration mode of OH is presented by a distinct peak at 3422 cm^{-1} while the Fe–O stretch appear as large band at 554 cm^{-1}. The presence of hydroxyl functional groups on the nanoparticle surface can be responsible for the negative surface charge of the MNP.

The surface charge of the magnetite nanoparticles is strongly dependent on the pH value (surface OH groups). At low pH, the surface is protonated therefore it is positively charged, while it becomes deprotonated at high pH. The hydroxyl groups on the surface of MNP have amphoteric character; they can act either as acids or bases.[32] Finally, the presence of the functional groups (mainly –OH) lead to proper dispersibility in aqueous phase and hydrogen bond formation between nanoparticles and DNA. The lowest value (> −18 mV) was found in case of the A1 sample (Figure 6A). This sample has the smallest size as well (15.3 nm) and thus, it is considered as the best sample for DNA purification (high surface area and great dispersibility).

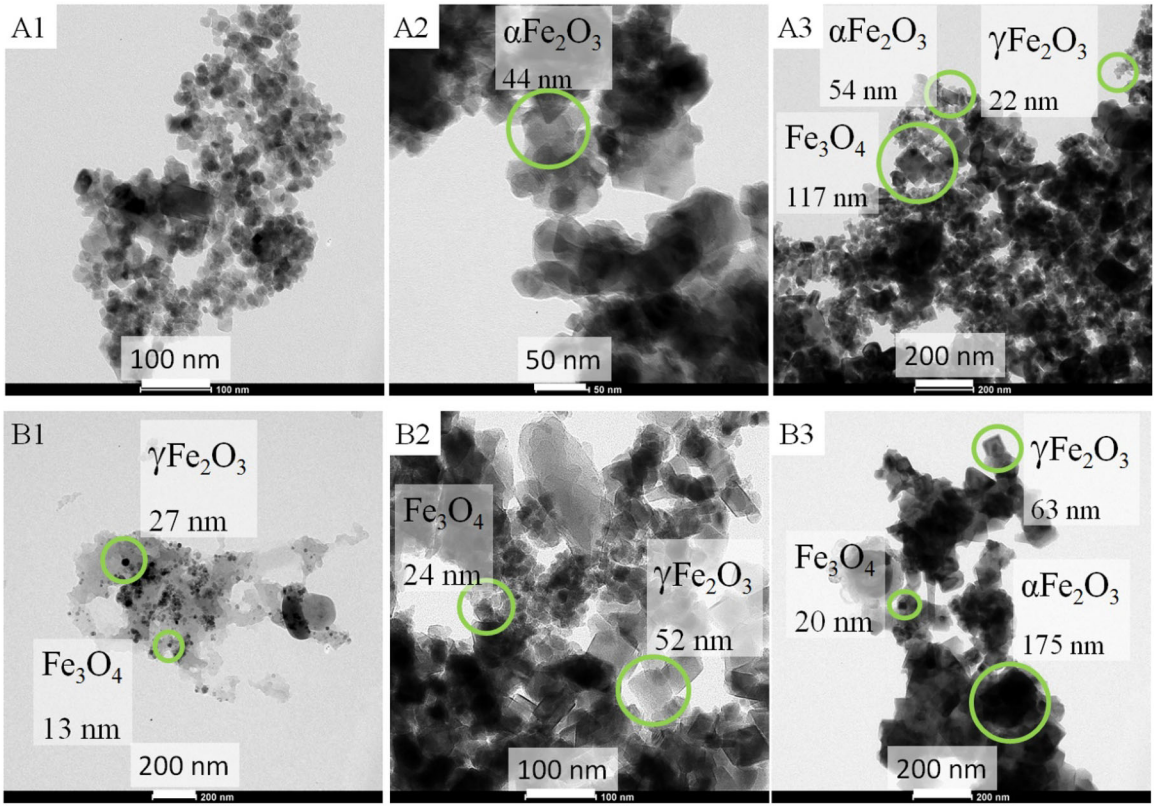

Figure 5. High-resolution transmission electron microscopy (HRTEM) images of the synthesized iron oxide nanoparticles. The identified phases also noted with green circles.

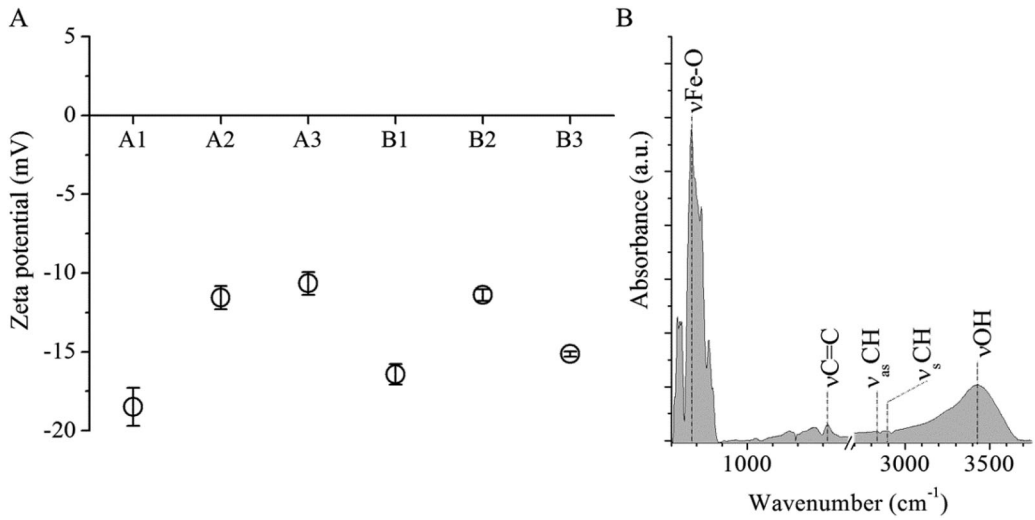

Figure 6. Zeta potentials of the iron oxide samples (A), FTIR spectra of A1 sample (B).

DNA binding capacity test

Gel electrophoresis experiments have been carried out to test the success of reversible DNA-MNP binding. In Figure 7 the first well of the agarose gel contains the DNA sample purified from *E. coli* and its characteristic band is considered as positive control (Well 1). No DNA related signal was found (see Well 3 of Figure 7) in the supernatant of the DNA-MNP mixture, while the results from the two elution fractions of the DNA-MNP gave a band at the same molecular weight as positive (see Well 5 and 7 represent the first and the second elution fraction, respectively). This can be assigned to the eluted DNA proving that the DNA could reversibly bind to the MNP. As the agarose gel image shows, the major amount of the DNA was eluted in the first step (Well 5), and the remaining DNA can be eluted during the second elution step (Well 7). The additional band of the elution fractions might be due to the DNA aggregation leading to larger MW. DNA-free MNP sample (A1 sample) was used as negative control in the DNA binding capacity tests, in which ultrapure water was used instead of DNA. No band was found for DNA-free sample at any steps of the binding capacity test (Well 4, 6, and 8 represent the

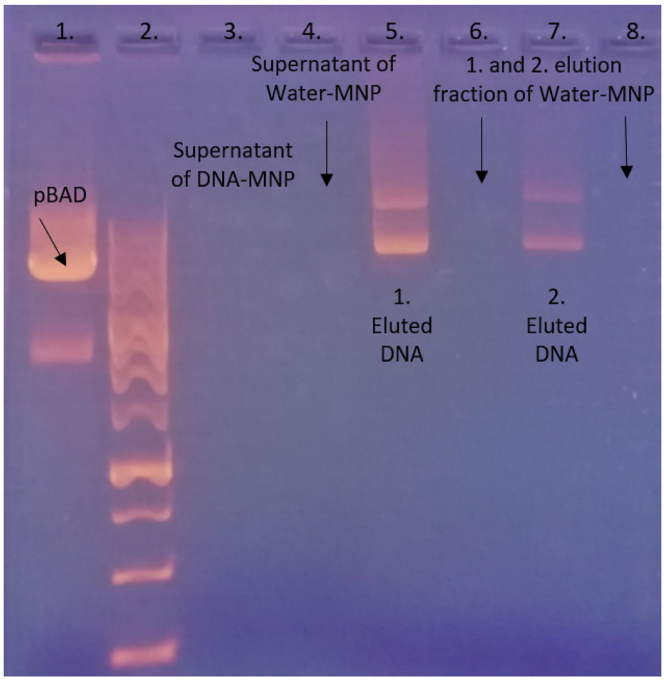

Figure 7. Gel electrophoresis image: (1) Purified pBAD type plasmid DNA (Positive control); (2) 1 kb DNA ladder (cat. No.: CEB-P-0107-250); (3) Supernatant of the DNA-MNP mixture; (4) Supernatant of the MNP-ultra-pure water mixture (negative control); (5) Supernatant of the DNA-MNP mixture after elution (eluted DNA); (6) Supernatant of the MNP-ultra-pure water mixture (negative control); (7) Sample taken from the second elution of the DNA-MNP mixture (eluted DNA); 8: Supernatant of the MNP-ultra-pure water mixture (negative control).

supernatant of the ultrapure water-MNP mixture, the first elution and the second elution fraction of the DNA-free sample, respectively). These results demonstrate that the noticed fluorescent bands on the agarose gel image unambiguously belongs to the reversibly bound and eluted DNA. As reference 1 kb DNA molecular size marker was used during the electrophoresis (Well 2).

Conclusions

We have successfully produced iron oxide magnetic nanoparticles (MNP) using a newly developed, combined sono-chemical-combustion procedure. Two different iron precursors, ferrocene and iron(II)-acetate and three polyethylene-glycol dispersants with different molecular weight (PEG 200, 600, and 1000) were used to synthesize the nanoparticles. Three crystalline forms (three phases) of iron oxides were identified: hematite, magnetite, and maghemite. By changing the iron precursor and the molecular weight of the dispersant, the ratio of the iron oxide phases can be tuned. Due to the relatively large negative electrokinetic potential the dispersion of these MNPs is kinetically stable in aqueous phase. In addition, DNA-MNP binding tests shown that the initially purified DNA interacted with the MNP, thus there was no detectable DNA in the supernatant of the DNA-MNP mixture. DNA was shown only in the elution fraction. It means that DNA molecule first bound to the tested nanoparticles and then the DNA molecules redissolved into the elution fraction when the binding buffer was replaced by highly purified water. This is an important phenomenon, because it enables the usage of these MNP in DNA purification processes (e.g. in case of complex samples). If DNA molecules are eluted completely from the surface of the MNP, the same nanoparticles can be applicable again for further purification/binding processes. In this work it has been revealed that the synthesized superparamagnetic nanoparticles can be applicable without further surface functionalization in processes where binding of DNA molecules is necessary.

Acknowledgements

The EFOP-3.6.1-16-2016-00014 project is also gratefully acknowledged due to support our work.

Disclosure statement

Conflict of interest on behalf of all authors, the corresponding author states that there is no conflict of interest.

Funding

This research was supported by the European Union and the Hungarian State, co-financed by the European Regional Development Fund in the framework of the GINOP-2.3.4-15-2016-00004 project, aimed to promote the cooperation between the higher education and the industry 00004 project, aimed to promote the cooperation between the higher education and the industry.

ORCID

László Vanyorek http://orcid.org/0000-0002-0630-0595

References

[1] Singh, H.; Du, J.; Singh, P.; Mavlonov, G. T.; Yi, T. H. Development of Superparamagnetic Iron Oxide Nanoparticles via Direct Conjugation with Ginsenosides and Its in-Vitro Study. *J. Photochem. Photobiol. B Biol.* **2018**, *185*, 100–110. DOI: 10.1016/j.jphotobiol.2018.05.030.

[2] Massart, R. Preparation of Aqueous Magnetic Liquids in Alkaline and Acidic Media. *IEEE Trans. Magn.* **1981**, *17*, 1247–1248. DOI: 10.1109/TMAG.1981.1061188.

[3] Park, J.; Lee, E.; Hwang, N.-M.; Kang, M.; Kim, S. C.; Hwang, Y.; Park, J.-G.; Noh, H.-J.; Kim, J.-Y.; Park, J.-H.; Hyeon, T. One-Nanometer-Scale Size-Controlled Synthesis of Monodisperse Magnetic Iron Oxide Nanoparticles. *Angew. Chem. Int. Ed.* **2005**, *44*, 2872–2877. DOI: 10.1002/anie.200461665.

[4] Wu, W.; Wu, Z.; Yu, T.; Jiang, C.; Kim, W.-S. Recent Progress on Magnetic Iron Oxide Nanoparticles: synthesis, Surface Functional Strategies and Biomedical Applications. *Sci. Technol. Adv. Mater.* **2015**, *16*, 023501. DOI: 10.1088/1468-6996/16/2/023501.

[5] Farahmandjou, M.; Soflaee, F. Synthesis and Characterization of α-Fe2O3 Nanoparticles by Simple co-Precipitation Method. *Phys. Chem. Res.* **2015**, *3*, 191–196. DOI: 10.22036/pcr.2015.9193.

[6] Soflaee, F.; Farahmandjou, M.; Firoozabadi, T. P. Polymer-Mediated Synthesis of Iron Oxide (Fe2O3) Nanorod. *Chinese J. Phys.* **2015**, *53*, 1–9. DOI: 10.6122/CJP.20150413.

[7] Majid, F.; Soflaee, F. Low Temperature Synthesis of α-Fe2O3 Nano-Rods Using Simple Chemical Route. *J. Nanostructures* **2014**, *4*, 413–418. DOI: 10.7508/jns.2014.04.002.

[8] Farahmandjoua, M.; Honarbakhsha, S.; Behrouziniab, S. PVP-Assisted Synthesis of Cobalt Ferrite (CoFe2O4) Nanorods. *Phys. Chem. Res.* **2016**, *4*, 655–662. DOI: 10.22036/pcr.2016.16702.

[9] Farahmandjou, M.; Soflaee, F. Synthesis of Iron Oxide Nanoparticles Using Borohydride Reduction. *Int. J. Bio-Inorganic Hybrid Nanomater.* **2014**, *3*, 203–206.

[10] Wongwailikhit, K.; Horwongsakul, S. The Preparation of Iron (III) Oxide Nanoparticles Using W/O Microemulsion. *Mater. Lett.* **2011**, *65*, 2820–2822. DOI: 10.1016/j.matlet.2011.05.063.

[11] Prathna, T. C.; Mathew, L.; Chandrasekaran, N.; Raichur, A. M.; Mukherjee, A. Biomimetic Synthesis of Nanoparticles: Science, Technology & Applicability. In: *Biomimetics Learn from Nat*. InTech, **2010**. DOI: 10.5772/8776.

[12] Pascal, C.; Pascal, J. L.; Favier, F.; Elidrissi Moubtassim, M. L.; Payen, C. Electrochemical Synthesis for the Control of γ-Fe_2O_3 Nanoparticle Size. Morphology, Microstructure, and Magnetic Behavior. *Chem. Mater.* **1999**, *11*, 141–147. DOI: 10.1021/cm980742f.

[13] Starowicz, M.; Starowicz, P.; Żukrowski, J.; Przewoźnik, J.; Lemański, A.; Kapusta, C.; Banaś, J. Electrochemical Synthesis of Magnetic Iron Oxide Nanoparticles with Controlled Size. *J. Nanopart. Res.* **2011**, *13*, 7167–7176. DOI: 10.1007/s11051-011-0631-5.

[14] Wang, G.; Ling, Y.; Wheeler, D. A.; George, K. E. N.; Horsley, K.; Heske, C.; Zhang, J. Z.; Li, Y. Facile Synthesis of Highly Photoactive α-Fe2O3 -Based Films for Water Oxidation. *Nano Lett.* **2011**, *11*, 3503–3509. DOI: 10.1021/nl202316j.

[15] Pang, Y. L.; Lim, S.; Ong, H. C.; Chong, W. T. Research Progress on Iron Oxide-Based Magnetic Materials: Synthesis Techniques and Photocatalytic Applications. *Ceram. Int.* **2016**, *42*, 9–34. DOI: 10.1016/j.ceramint.2015.08.144.

[16] Ramli, N. I. T.; Rashid, S. A.; Mamat, M. S.; Sulaiman, Y.; Krishnan, S. Incorporation of Iron Oxide into CNT/GNF as a High-Performance Supercapacitor Electrode. *Mater. Chem. Phys.* **2018**, *212*, 318–324. DOI: 10.1016/j.matchemphys.2018.03.044.

[17] Liu, R.; Guo, Y.; Odusote, G.; Qu, F.; Priestley, R. D. Core–Shell Fe_3O_4 Polydopamine Nanoparticles Serve Multipurpose as Drug Carrier, Catalyst Support and Carbon Adsorbent. *ACS Appl. Mater. Interfaces* **2013**, *5*, 9167–9171. DOI: 10.1021/am402585y.

[18] Brebu, M.; Azhar Uddin, M.; Muto, A.; Sakata, Y.; Vasile, C. Catalytic Degradation of Acrylonitrile – Butadiene – Styrene into Fuel Oil 1. The Effect of Iron Oxides on the Distribution of Nitrogen-Containing Compounds. *Energy Fuels* **2001**, *15*, 559–564. DOI: 10.1021/ef000124x.

[19] Amstad, E.; Zurcher, S.; Mashaghi, A.; Wong, J. Y.; Textor, M.; Reimhult, E. Surface Functionalization of Single Superparamagnetic Iron Oxide Nanoparticles for Targeted Magnetic Resonance Imaging. *Small* **2009**, *5*, 1334–1342. DOI: 10.1002/smll.200801328.

[20] Yang, H.; Zhuang, Y.; Sun, Y.; Dai, A.; Shi, X.; Wu, D.; Li, F.; Hu, H.; Yang, S. Targeted Dual-Contrast T1- and T2-Weighted Magnetic Resonance Imaging of Tumors Using Multifunctional Gadolinium-Labeled Superparamagnetic Iron Oxide Nanoparticles. *Biomaterials* **2011**, *32*, 4584–4593. DOI: 10.1016/j.biomaterials.2011.03.018.

[21] Yu, C. H.; Al-Saadi, A.; Shih, S.-J.; Qiu, L.; Tam, K. Y.; Tsang, S. C. Immobilization of BSA on Silica-Coated Magnetic Iron Oxide Nanoparticle. *J. Phys. Chem. C.* **2009**, *113*, 537–543. DOI: 10.1021/jp809662a.

[22] Chandra Mohanta, S.; Saha, A.; Sujatha Devi, P. PEGylated Iron Oxide Nanoparticles for pH Responsive Drug Delivery Application. *Mater. Today Proc.* **2018**, *5*, 9715–9725. DOI: 10.1016/j.matpr.2017.10.158.

[23] Ayala, V.; Herrera, A. P.; Latorre-Esteves, M.; Torres-Lugo, M.; Rinaldi, C. Effect of Surface Charge on the Colloidal Stability and in Vitro Uptake of Carboxymethyl Dextran-Coated Iron Oxide Nanoparticles. *J. Nanopart. Res.* **2013**, *15*, 1874.DOI: 10.1007/s11051-013-1874-0.

[24] Yue-Jian, C.; Juan, T.; Fei, X.; Jia-Bi, Z.; Ning, G.; Yi-Hua, Z.; Ye, D.; Liang, G. Synthesis, Self-Assembly, and Characterization of PEG-Coated Iron Oxide Nanoparticles as Potential MRI Contrast Agent. *Drug Dev. Ind. Pharm.* **2010**, *36*, 1235–1244. DOI: 10.3109/03639041003710151.

[25] Sosa-Acosta, J.; Silva, J. A.; Fernández-Izquierdo, L.; Díaz-Castañón, S.; Ortiz, M.; Zuaznabar-Gardona, J. C.; Díaz-García, A. M. Iron Oxide Nanoparticles (IONPs) with Potential Applications in Plasmid DNA Isolation. *Colloids Surfaces A Physicochem. Eng. Asp.* **2018**, *545*, 167–178. DOI: 10.1016/j.colsurfa.2018.02.062.

[26] Oberacker, P.; Stepper, P.; Bond, D. M.; Höhn, S.; Focken, J.; Meyer, V.; Schelle, L.; Sugrue, V. J.; Jeunen, G.-J.; Moser, T.; et al. Bio-On-Magnetic-Beads (BOMB): Open Platform for High-Throughput Nucleic Acid Extraction and Manipulation. *PLOS Biol.* **2019**, *17*, e3000107. DOI: 10.1371/journal.pbio.3000107.

[27] Kang, K.; Choi, J.; Nam, J. H.; Lee, S. C.; Kim, K. J.; Lee, S.-W.; Chang, J. H. Preparation and Characterization of Chemically Functionalized Silica-Coated Magnetic Nanoparticles as a DNA Separator. *J. Phys. Chem. B.* **2009**, *113*, 536–543. DOI: 10.1021/jp807081b.

[28] Tanaka, T.; Sakai, R.; Kobayashi, R.; Hatakeyama, K.; Matsunaga, T. Contributions of Phosphate to DNA Adsorption/Desorption Behaviors on Aminosilane-Modified Magnetic Nanoparticles. *Langmuir* **2009**, *25*, 2956–2961. DOI: 10.1021/la8032397.

[29] Ghaemi, M.; Absalan, G. Study on the Adsorption of DNA on Fe3O4 Nanoparticles and on Ionic Liquid-Modified Fe3O4 Nanoparticles. *Microchim. Acta.* **2014**, *181*, 45–53. DOI: 10.1007/s00604-013-1040-5.

[30] Hawkins, T. L.; O'Connor-Morin, T.; Roy, A.; Santillan, C. DNA Purification and Isolation Using a Solid-Phase. Nucl. Acids *Res.* **1994**, *22*, 4543–4544. DOI: 10.1093/nar/22.21.4543.

[31] Saiyed, Z. M.; Bochiwal, C.; Gorasia, H.; Telang, S. D.; Ramchand, C. N. Application of Magnetic Particles (Fe3O4) for Isolation of Genomic DNA from Mammalian Cells. *Anal. Biochem.* **2006**, *356*, 306–308. DOI: 10.1016/j.ab.2006.06.027.

[32] Moacă, E.-A.; Coricovac, E. D.; Soica, C. M.; Pinzaru, I. A.; Păcurariu, C. S.; Dehelean, C. A. Preclinical Aspects on Magnetic Iron Oxide Nanoparticles and Their Interventions as Anticancer Agents: Enucleation, Apoptosis and Other Mechanism, in: Iron Ores Iron Oxide Mater. *InTech.* **2018**. DOI: 10.5772/intechopen.74176.